Inorg. Chem. **2008**, *47*, 6756−6762

High-Pressure Anisotropic Distortion of $Pb_3Bi_2S_6$: a Pressure-Induced, Reversible Phase Transition with Migration of Chemical Bonds

Lars A. Olsen,* Tonči Balić-Žunić, and Emil Makovicky

Department of Geography and Geology, University of Copenhagen, Øster Voldgade 10, 1350 Copenhagen K, Denmark

Received February 28, 2008

The compound $Pb_3Bi_2S_6$ is investigated by X-ray diffraction on single crystals in a diamond-anvil cell between 0.0001 and 10.5 GPa. It undergoes a first-order phase transition at hydrostatic pressure between 3.7 and 4.9 GPa. The space group symmetry changes from *Bbmm* to *Pbnm*, and the unit-cell volume decreases by 4%. The transition is strongly anisotropic, with a contraction along one of the crystal axes by 16% and expansion along another one by 14%. This is a piezoplastic phase transition, a displacive pressure-induced phase transition with systematic shearing of atomic planes and a migration of chemical bonds in the structure. In the case of $Pb_3Bi_2S_6$ the transition is achieved by the change of the archetypal architecture of the structure-building modules from a PbS-like to a SnS-like arrangement and a loss of mirror planes on the contact surfaces of modules. The phase transition is reversible with a preservation of the single crystal, which is a result of the stereochemical influence and migration of the s^2 lone electron pairs of Pb^{II} and Bi^{III}.

Introduction

A number of complex structures can be shown to be of a modular character. They are composed of modules with a relatively simple archetypal structure, combined by symmetry or pseudosymmetry operations.[1] The large family of sulfosalts, complex sulfides of As^{III}, Sb^{III}, Bi^{III}, or Te^{IV}[2] presents many examples of modular structures of variable complexity. Their modules are based on the NaCl/PbS archetype or its systematic distortions and cover therefore interesting variations of structure types based on octahedral and higher-number coordinations. Some of them are therefore interesting as low-pressure equivalents for the high-pressure silicate phases of the Earth's interior, which are based on the octahedrally coordinated silicon in combination with other cations with the same or higher coordination number (CN). An example of the relation of sulfosalts to the high-pressure silicates is the postperovskite phase of $MgSiO_3$[3,4] which belongs to the same homologous series of structure types as the lillianite ($Pb_3Bi_2S_6$) investigated in this work. Sulfosalts can have interesting semiconducting and ion-conducting properties because of the nature of the metalloid–sulfur bond, variable chemical composition due to complex atom-substitution schemes, and the presence of the s^2 lone-electron pair (LEP) of metalloids and some typical accompanying cations (like Pb^{II} and Tl^{I}). Their potential use in solar cells and other technical applications is being investigated.[5,6]

The nonbonding LEPs of cations in sulfosalts are often stereochemically active, which is reflected in local distortions of the archetypal structure of modules. The distortion of the simple PbS/NaCl-like archetype can be systematic and lead to a new archetype (SnS) characterized by CN 7 rather than CN 6, which is reflected also in the classification schemes of the sulfosalt families.[7,8] Our group is currently investigating the high-pressure behavior of sulfosalts to get a better understanding of the changes in the LEP stereochemical activity under compression, a subject which attracts increased

* To whom correspondence should be addressed. E-mail: lao@geol.ku.dk.

(1) Ferraris, G.; Makovicky, E.; Merlino, S. *Crystallography of Modular Materials*; IUCr Monographs on Crystallography 15; Oxford University Press: Oxford, 2004.
(2) Moëlo, Y.; Makovicky, E. *Eur. J. Mineral.* **2008**, *20*, 7–46.
(3) Murakami, M.; Hirose, K.; Kawamura, K.; Sata, N.; Ohishi, Y. *Science* **2004**, *304*, 855–858.
(4) Oganov, A. R.; Ono, S. *Nature* **2004**, *430*, 445–448.
(5) Dittrich, H.; Bieniok, A.; Brendel, U.; Grodzicki, M.; Topa, D. *Thin Solid Films* **2007**, *515*, 5745–5750.
(6) Kryukova, G. N.; Heuer, M.; Wagner, G.; Doering, T.; Bente, K. *J. Solid State Chem.* **2005**, *178*, 376–381.
(7) Makovicky, E.; Mumme, W. G. *Z. Kristallogr.* **1981**, *154*, 236–238.
(8) Makovicky, E. *Fortschr. Mineral.* **1985**, *63*, 45–89.

10.1021/ic800380p CCC: $40.75
Published on Web 06/28/2008

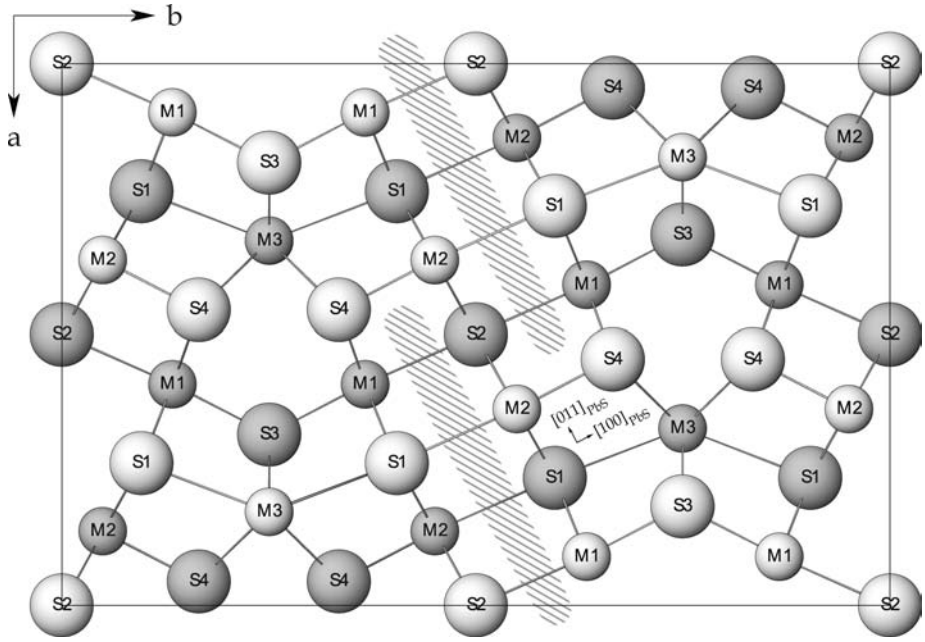

Figure 1. One unit cell from the crystal structure of lillianite. Gray circles represent atoms on the $z = 0.25$ mirror plane, white circles represent atoms on the $z = 0.75$ mirror plane. The orientation of the PbS-archetype axes inside one (010) structural slab is indicated. Cores of the LEP micelles are indicated by ruling.

interest in the high-pressure research.[9] The present investigation reveals a decisive effect of the LEP on the high-pressure phase transition of a kind which, to the best of our knowledge, has not been observed before.

The crystal structure of low-pressure $Pb_3Bi_2S_6$ (lillianite) is orthorhombic *Bbmm*.[10,11] Its moduli are the alternating layers with PbS-archetype internal structure, with surfaces cut parallel to $(311)_{PbS}$, and combined on these surfaces by mirror planes parallel to (010) (Figure 1). Lillianite belongs to a homologous series of structures built on the same basic principle. Individual homologues vary by the width of the PbS-like modules (layers) which is expressed as the number N of octahedra running diagonally across an individual slab parallel to $[011]_{PbS}$. Each lillianite homologue is denoted as ^{N_1,N_2}L, where N_1 and N_2 are N values for two adjacent mirror-related layers.[12] Thus, lillianite is the homologue ^{4,4}L of this accretional series.

Experimental Section

A synthetic single-crystal ($120 \times 60 \times 40\ \mu m^3$) of lillianite was mounted in a Diacell DXR-6 (now Diacell Bragg-(S)) diamond anvil cell (DAC) inside a 200 μm hole in a stainless steel gasket preindented to a thickness of 90 μm. A mixture of methanol:ethanol:water = 16:3:1 which is hydrostatic up to the maximum pressure reached in this work[13] was used as a pressure-transmitting medium. The unit-cell volume of a single crystal of quartz[14] was used for pressure calibration. X-ray diffraction intensities were collected at 298 K using graphite-monochromatized Mo Kα radiation on a CCD-equipped Bruker AXS four-circle diffractometer. Pressure was stepwise increased to 10.5 GPa and after each compression step the crystal was given at least 12 h rest time before the measurement. X-ray diffraction intensities of the same crystal were also collected at room pressure before and after the DAC experiment. Because of its small size and inconvenient orientation in the DAC, the crystal gave diffraction intensities of inferior quality for structure refinement. Therefore, a second lillianite crystal ($150 \times 65 \times 50\ \mu m^3$) was selected from the same synthetic batch, and the DAC experiment was repeated between 0 and 7.9 GPa. The structure refinement of this crystal gave satisfactory residuals. The abbreviations *lill1* and *lill2* are used to refer to the first and second crystal, respectively.

The orientation and the preliminary dimensions of the unit cell, as prerequisites for intensity integration, were obtained using the program SMART. Intensity integration was carried out using the SAINT+ software. Both programs are products of Bruker-AXS. Weak lillianite reflections overlapping with the strongest powder diffraction ring from the beryllium backing plates were rejected by a filtering routine. Lillianite reflections overlapping with diamond reflections were rejected manually after visual inspection of the collected CCD frames. Absorption corrections were made with the Absorb6.1 program.[15] SHELXL-97[16] was used for structure refinement. Geometrical analyses were made with IVTON.[17]

Results and Discussion

The evolution of the unit-cell parameters of $Pb_3Bi_2S_6$ with pressure (Tables 1 and 2, Figure 2) shows an abrupt change between 3.7 and 4.9 GPa. The unit cell has an almost perfect isotropic compression between 0 and 3.7 GPa. The relative compression $l_{3.7}/l_0$, where l is the axis length and the subscript

(9) Grzechnik, A. In *Pressure-Induced Phase Transitions*; Grzechnik, A., Ed.; Transworld Research Network: Kerala, India, 2007.
(10) Otto, H. H.; Strunz, H. *Neues Jahrb. Mineral., Abh.* **1968**, *108*, 1–19.
(11) Takagi, J.; Takéuchi, Y. *Acta Crystallogr., Sect. A* **1972**, *28*, 649–651.
(12) Makovicky, E.; Karup-Møller, S. *N. Jb. Miner. Abh.* **1977**, *130*, 264–287.
(13) Angel, R.; Bujak, M.; Zhao, J.; Gatta, G. D.; Jacobsen, S. D. *J. Appl. Crystallogr.* **2007**, *40*, 26–32.
(14) Angel, R.; Allan, D.; Miletich, R.; Finger, L. *J. Appl. Crystallogr.* **1997**, *30*, 461–466.
(15) Angel, R. J. *J. Appl. Crystallogr.* **2004**, *37*, 486–492.
(16) Sheldrick, G. M. *Acta Cryst. A* **2008**, *64*, 112–122.
(17) Balić-Žunić, T.; Vikoić, I. *J. Appl. Crystallogr.* **1996**, *29*, 305–306.

Table 1. Unit-Cell Parameters of $Pb_3Bi_2S_6$ *lill1* Crystal at Different Pressures[a]

P (GPa)	a (Å)	b (Å)	c (Å)	V (Å^3)
0.0001	13.528(4)	20.632(6)	4.1145(10)	1148.4(5)
1.03(4)	13.444(1)	20.493(4)	4.0876(5)	1126.2(3)
1.33(4)	13.419(1)	20.447(4)	4.0801(4)	1119.6(3)
2.13(4)	13.349(1)	20.346(3)	4.0623(4)	1103.4(3)
2.73(4)	13.301(1)	20.272(3)	4.0504(4)	1092.1(3)
4.92(4)	11.051(2)	23.083(5)	4.0332(6)	1028.8(4)
5.49(3)	11.022(1)	22.992(5)	4.0261(6)	1020.3(4)
6.42(4)	10.977(1)	22.858(4)	4.0125(5)	1006.8(3)
7.12(3)	10.942(1)	22.766(4)	4.0042(5)	997.5(3)
7.63(4)	10.918(1)	22.707(4)	3.9993(5)	991.5(3)
8.55(3)	10.882(1)	22.606(4)	3.9887(5)	981.3(3)
8.84(3)	10.877(1)	22.590(4)	3.9857(5)	979.3(3)
10.48(3)	10.816(1)	22.424(4)	3.9663(5)	962.0(3)

[a] All data points are measured during compression.

indicates pressure, is 0.977 for the *a*-axis. The corresponding values for the *b*- and *c*-axes are 0.977 and 0.979, respectively. Between 3.7 and 4.9 GPa, the length of the *a*-axis decreases by 16%, the *b*-axis increases by 14%, while the *c*-axis maintains a length of 4.03 Å. The bulk result is a contraction of the unit-cell volume from 1073.9 Å^3 to 1028.8 Å^3, corresponding to 4%. At pressures higher than 4.9 GPa the rate of compression differs for each unit-cell axis. The long *b*-axis becomes the most compressible one while the short *c*-axis shows the least relative compression. The ratios $l_{10.5}/l_{4.9}$ are 0.979, 0.971, and 0.983 for the *a*-, *b*-, and *c*-axes, respectively.

The bulk modulus K_0 and its first pressure derivative K' were determined by fitting an equation of state (EoS) to the unit-cell volumes. For the unit-cell volumes between 0 and 3.7 GPa a third-order Birch−Murnaghan (BM3) EoS[18] with fixed V_0 (1148.4 Å^3) yields a $K_0 = 48.6(1.6)$ GPa and $K' = 3.9(1.2)$. With all three parameters released for refinement and the data points weighted by estimated standard deviations of volume and pressure, a fitted BM3 EoS yields $V_0 = 1148.5(3)$ Å^3, $K_0 = 48.4(1.7)$ GPa, and $K' = 4.0(1.3)$. The value obtained for K' might be influenced by the limited pressure interval. Lillianite shows the largest K_0 and the smallest K' values among the sulfosalts and sulfides of metalloids studied so-far,[19–21] the others having K_0 values from 26.9 to 43.9 GPa and K' values from 6.4 to 7.9.

As realized by Olsen et al.[19] the bulk modulus of galenobismutite ($PbBi_2S_4$), $K_0 = 43.9(7)$ GPa, corresponds to a sum of moduli of Bi_2S_3 (36.6 GPa[20]) and PbS (51.0 GPa[22]) weighted according to molar proportions. From an equivalent equation, $K_{Pb3Bi2S6} = (K_{Bi2S3} + 3K_{PbS})/4$, a bulk modulus of 47.4 GPa is obtained for lillianite, close to the experimental value of 48.4(1.7) GPa. This interesting result, apparently little dependent on the structure types involved but possibly characteristic for the specific type of bonding in these compounds, still awaits an exact explanation.

For the high-pressure phase, hereafter called β-$Pb_3Bi_2S_6$, the method of self-similarity as described by Angel[23] is employed. The fitting of a BM3 EoS yields the following parameters: $V_{4.9} = 1028.8(7)$ Å^3, $K_{4.9} = 63.8(3.0)$ GPa, and $K' = 8.1(1.0)$ where the subscript indicates the reference pressure in GPa.

Two crystals labeled *lill1* and *lill2* have been investigated. For the crystal structure refinement only the data from the *lill2* crystal have been used, because *lill1*, due to the small size and inconvenient orientation in the DAC, gave diffraction intensities of inferior quality. Experimental conditions for the six measurements used for the structure refinement are presented in Table 2. Four data points fall into the field of stability of lillianite, and the last two represent β-$Pb_3Bi_2S_6$.

The crystal structure of lillianite has three distinct cation positions of which two (M1, M2) are situated in octahedral coordinations inside the PbS-archetype slab (Figure 1). The third metal site (M3) is positioned at the boundary of the slabs and coordinated by a bicapped trigonal prism of sulfurs (CN 8). The degree of Pb−Bi order in lillianite has been much discussed, because it is practically impossible to distinguish these atoms by X-ray diffraction as a result of their similar and high atomic numbers. M3 is assumed to be a fully occupied Pb-position while M1 and M2 are mixed Pb,Bi sites. It has been put forward that there is a preference for Pb in M1 and for Bi in M2 (see ref 24 for a detailed discussion).

The refined atomic coordinates for lillianite are given in Table 3, whereas the atomic displacement factors can be found in Table 4. The atomic displacements were refined anisotropically for M atoms and isotropically for sulfur atoms. Table 5 presents the bond lengths at room pressure and at the highest measured pressure (3.73 GPa) before the phase transition.

The LEPs of Pb and Bi in lillianite show a mild stereochemical activity in the variation of bond distances. An active LEP is orientated opposite to the shortest bond(s) in the polyhedron. The LEPs of M1 and M2 are hosted in a LEP micelle (for a definition of a LEP micelle, see ref 25) in the center of the PbS slab (Figure 1, Table 5). The level of LEP activity can be quantified by the cation eccentricity which measures the displacement of the cation from the centroid of the polyhedron.[26] For the three distinct cation sites in lillianite, eccentricities are shown in Figure 3. They are consistent with the proposed attribution of the site occupancies and the expected larger activity of the Bi^{III} LEP. The eccentricities are generally lower than those in galenobismutite ($PbBi_2S_4$[19]) which range 0.08−0.12 or those in bismuthinite (Bi_2S_3[20]) which show values of about 0.15, also in accordance with a higher Pb/Bi ratio in lillianite.

The cation eccentricity of the M3 site, situated between the PbS-archetype slabs, decreases markedly from its already

(18) Birch, F. *Phys. Rev.* **1947**, *11*, 809–824.
(19) Olsen, L. A.; Balić-Žunić, T.; Makovicky, E.; Ullrich, A.; Miletich, R. *Phys. Chem. Miner.* **2007**, *34*, 467–475.
(20) Lundegaard, L. F.; Makovicky, E.; Boffa-Ballaran, T.; Balić-Žunić, T. *Phys. Chem. Miner.* **2005**, *32*, 578–584.
(21) Lundegaard, L. F.; Miletich, R.; Balić-Žunić, T.; Makovicky, E. *Phys. Chem. Miner.* **2003**, *30*, 463–468.
(22) Knorr, K.; Ehm, L.; Hytha, M.; Winkler, B.; Depmeier, W. *Eur. Phys. J. B* **2003**, *31*, 297–303.
(23) Angel, R. J. *Rev. Mineral. Geochem.* **2000**, *41*, 35–60.
(24) Pinto, D.; Balić-Žunić, T.; Garavelli, A.; Makovicky, E.; Vurro, F. *Can. Mineral.* **2005**, *44*, 159–175.
(25) Makovicky, E.; Mumme, W. G. *Neues Jahrb. Mineral. Abh.* **1983**, *147*, 58–79.
(26) Balić-Žunić, T.; Makovicky, E. *Acta Crystallogr., Sect. B* **1996**, *52*, 78–81.

Table 2. Experimental Data For $Pb_3Bi_2S_6$ *lill2* Crystal[a].

P (GPa)	0.0001	1.95(4)	2.90(3)	3.73(3)	5.27(4)	7.92(5)
			Crystal Data			
a (Å)	13.540(3)	13.353(2)	13.280(2)	13.216(2)	11.026(4)	10.891(4)
b (Å)	20.637(4)	20.367(4)	20.260(4)	20.163(5)	23.023(8)	22.683(9)
c (Å)	4.1103(7)	4.0615(5)	4.0448(5)	4.0300(5)	4.0233(8)	3.9926(9)
V (Å^3)	1148.5(4)	1104.6(3)	1088.3(3)	1073.9(3)	1021.2(5)	986.4(5)
ρ (g/cm^3)	7.125	7.408	7.519	7.619	7.996	8.295
μ (mm^{-1})	75.40	78.40	79.57	80.64	84.62	87.79
			Data Collection			
# measured reflections	6296	2175	2158	2116	2742	2536
# unique reflections	1005	471	465	453	558	525
# observed reflections[b]	776	283	284	277	264	238
R_{int}	0.0640	0.1608	0.1716	0.1724	0.2164	0.2110
$2\theta_{max}$ (deg)	61.01	57.66	57.98	57.67	46.50	46.51
range of h,k,l	$-19 \le h \le 19$	$-15 \le h \le 15$	$-15 \le h \le 15$	$-15 \le h \le 15$	$-10 \le h \le 11$	$-10 \le h \le 10$
	$-27 \le k \le 29$	$-18 \le k \le 20$	$-17 \le k \le 19$	$-17 \le k \le 19$	$-19 \le k \le 22$	$-19 \le k \le 21$
	$-5 \le l \le 5$	$-5 \le l \le 5$	$-5 \le l \le 5$	$-5 \le l \le 5$	$-4 \le l \le 4$	$-4 \le l \le 4$
			Refinement			
R1 ($\lvert F_o \rvert > 4\sigma$)	0.0465	0.0766	0.0783	0.0770	0.0940	0.0943
wR2	0.1126	0.1905	0.1866	0.1941	0.2290	0.2426
GoF	1.144	0.925	0.930	0.944	1.034	1.030
# parameters	26	26	26	26	49	49

[a] All data points are measured during compression. [b] Criterion for observed reflections is $\lvert F_o \rvert > 4\sigma$.

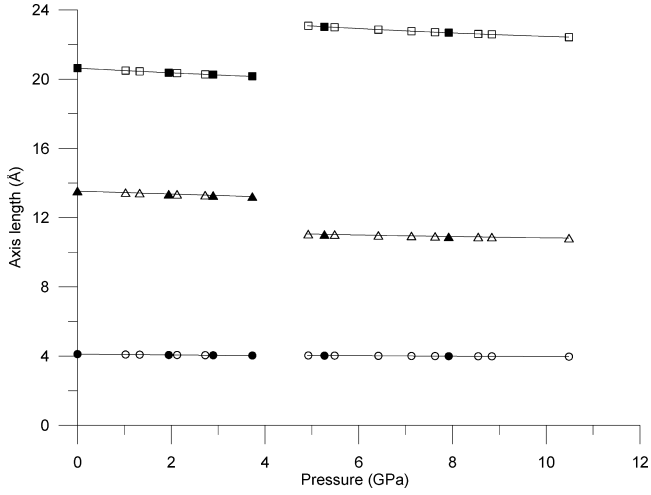

Figure 2. Evolution of unit-cell axes of $Pb_3Bi_2S_6$ with increasing pressure. Triangles indicate a, squares b, and circles c-axis. Void symbols represent the *lill1* crystal and filled symbols represent the *lill2* crystal.

low room-pressure value up to 2 GPa, but stabilizes at higher pressures. The LEPs of the two other cation sites, within the PbS-like slab, have a rigid respond to pressure throughout the stability range of lillianite. The stabilization of eccentricities between 2.9 and 3.7 GPa presages the phase transition by indicating that the structure has reached a limit of compressibility.

Between 3.7 and 4.9 GPa, lillianite transforms into the β-$Pb_3Bi_2S_6$ phase. It is a first-order phase transition with a marked change of both unit-cell volume and lengths of axes (Figure 2). The space group changes from *Bbmm* to *Pbnm* indicated by systematic extinctions in X-ray diffraction. In spite of the dramatic changes in unit-cell parameters, both investigated crystals still diffracted as single-crystals but with broadened reflections [a doubling of fwhm (full width at half maximum) on average]. After the pressure release the unit-cell parameters of the two crystals returned to the original room-pressure values and the lillianite structure type was re-established. As the reflections remained broad, we attribute the broadening to defects induced to the crystals by the dramatic phase transition.

Table 3. Atomic Coordinates for Lillianite (*lill2* Crystal)

P (GPa)		0.0001	1.95(4)	2.90(3)	3.73(3)
M1	x	0.09066(5)	0.08943(17)	0.08904(17)	0.08852(17)
	y	0.13373(3)	0.13374(13)	0.13358(13)	0.13359(13)
	z	0.50	0.50	0.50	0.50
M2	x	0.36273(4)	0.36196(17)	0.36155(17)	0.36091(18)
	y	0.04933(3)	0.04864(13)	0.04829(13)	0.04793(14)
	z	0.50	0.50	0.50	0.50
M3	x	0.32657(9)	0.3288(3)	0.3291(3)	0.3292(3)
	y	0.25	0.25	0.25	0.25
	z	0.00	0.00	0.00	0.00
S1	x	0.23628(37)	0.2359(12)	0.2341(11)	0.2341(12)
	y	0.09544(26)	0.0972(10)	0.0966(9)	0.0981(10)
	z	0.00	0.00	0.00	0.00
S2	x	0.00	0.00	0.00	0.00
	y	0.00	0.00	0.00	0.00
	z	0.50	0.50	0.50	0.50
S3	x	0.18371(45)	0.1821(17)	0.1804(17)	0.1787(17)
	y	0.25	0.25	0.25	0.25
	z	0.50	0.50	0.50	0.50
S4	x	0.45498(32)	0.4525(11)	0.4521(12)	0.4518(12)
	y	0.16496(22)	0.1687(9)	0.1684(9)	0.1684(9)
	z	0.50	0.50	0.50	0.50

Table 4. Atomic Displacement Factors for Lillianite (*lill2* Crystal)[a]

P (GPa)		0.0001	1.95(4)	2.90(3)	3.73(3)
M1	U_{ef}	0.0140(2)	0.0186(7)	0.0176(7)	0.0160(7)
M2	U_{ef}	0.01283(19)	0.0181(7)	0.0172(7)	0.0163(7)
M3	U_{ef}	0.0371(4)	0.0312(11)	0.0272(10)	0.0249(11)
S1	U_{iso}	0.0236(10)	0.030(4)	0.024(4)	0.024(4)
S2	U_{iso}	0.0148(12)	0.027(5)	0.027(5)	0.030(6)
S3	U_{iso}	0.0133(11)	0.020(5)	0.019(5)	0.017(5)
S4	U_{iso}	0.0160(9)	0.018(3)	0.020(3)	0.018(3)

[a] U_{ef} is 1/3 of the trace of the orthogonalized U_{ij} tensor.

Figure 4. shows the high-pressure crystal structure after the phase transition. β-$Pb_3Bi_2S_6$ has lost the mirror planes perpendicular to the b-axis, present in lillianite. They are replaced by n-glide planes and the space group of the high-pressure phase is *Pbnm*. This structure shows the characteristics of the meneghinite structural family of sulfosalts.[8,27]

Table 5. Cation−Anion Distances (Å) in Lillianite

P (GPa)		0.0001	3.73(3)
M1	S3	2.710(3)	2.63(1)
	2 × S4	2.831(3)	2.80(1)
	2 × S1	2.956(4)	2.88(1)
	S2	3.020(1)	2.937(3)
	⟨M1−S⟩	2.894	2.82
M2	S4	2.694(4)	2.71(2)
	2 × S1	2.839(4)	2.81(1)
	2 × S2	2.952(1)	2.894(2)
	S1	3.274(6)	3.20(2)
	⟨M2−S⟩	2.925	2.89
M3	4 × S4	3.213(3)	3.07(1)
	2 × S3	2.822(4)	2.83(2)
	2 × S1	3.417(6)	3.31(2)
	⟨M3−S⟩	3.166	3.07

As a consequence of the lowering of symmetry, some atomic sites which are symmetry equivalent in lillianite, are divided in two groups of symmetry-independent sites in β-$Pb_3Bi_2S_6$. This is the case for the $M1_{lill}$ and $M2_{lill}$ sites which split into $M2_\beta$ and $M5_\beta$ and into $M1_\beta$ and $M3_\beta$, respectively (compare Figures 1 and 4). The coordinations change from octahedral to monocapped trigonal prismatic and the CNs from 6 to 7. The $M3_{lill}$ site remains unique ($M4_\beta$) with a change of coordination from bicapped trigonal prismatic to monocapped trigonal prismatic, and the CN is lowered from 8 to 7. Note that the trigonal prism in this case is a standing one contrasted to lying ones of the other M sites in Figure 4. The phase transition equalizes the CNs of all cation sites with an increase of the average CN in accordance with the structure compaction.

Atom positions for β-$Pb_3Bi_2S_6$ are given in Table 6, atomic displacement factors in Table 7, and the bond lengths in Table 8. The estimated standard deviations of parameters are higher for the high-pressure phase, which is understandable, because the number of the observed reflections did not change because of the limitations imposed by the high-pressure measurement, whereas the number of parameters is doubled because of the lowering of symmetry. Large variation in bond lengths is seen for the M1, M3 and M5 sites, whereas the M2 and M4 sites are more regular. As the pressure is further increased from 5.3 to 7.9 GPa the crystal structure of β-$Pb_3Bi_2S_6$ responds as composed of rigid rods surrounded by softer LEP micelles (Figure 5). The inter-rod bonds are more shortened relative to the intrarod bonds, what causes a decrease in the variation of bond lengths for the cation sites. This indicates that the compression of β-$Pb_3Bi_2S_6$ is at the expense of the LEP activity.

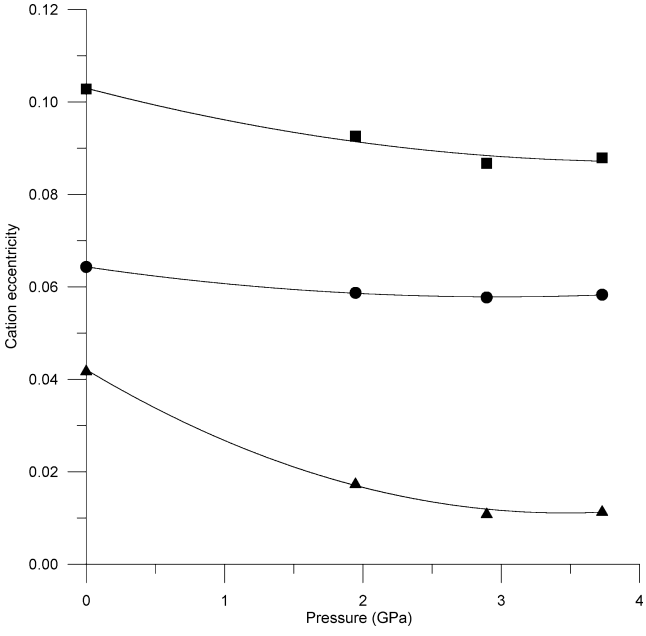

Figure 3. Cation eccentricities, defined according to ref 26, of lillianite between 0 and 4 GPa. Circles indicate M1; squares, M2; and triangles, M3 values.

The transition from lillianite to β-$Pb_3Bi_2S_6$ can be described by splitting the PbS-like slabs into rods parallel with the *c* axis by means of crystallographic shear (Figure 5). The rods are rotated around their central 2_1 axes, reducing the inclination angle of their longest diameter to the *b* axis. This leads to an expansion in the *b*-axis direction. Between 3.73 and 5.27 GPa the rotation amounts to 5°. Chemical bonds within the rods are shortened in β-$Pb_3Bi_2S_6$ in connection with the migration of LEPs to the inter-rod spaces. At the same time, the adjacent surfaces of neighboring rods are packed closer and this, together with the thinning of rods, contributes to a significant contraction along the *a* axis. The rotation is connected with a sliding of the adjacent rods. The relative movement between two parallel rods corresponds approximately to half an octahedron or the sliding component $[0\ ^1/_2\ ^1/_2\ ]_{PbS}$. The consequence is the migration of inter-rod bonds, seen in Figure 5. Moreover, the geometry of the inter-rod packing has changed because of displacement, and in this part, the coordinations of cations do not any more represent half-octahedra but rather lying trigonal prisms. The kind of systematic shear described above is characteristic for the relation between the PbS/NaCl and SnS archetype-structures.[7] In the language of the modular description of crystal structures, the phase transition changes the archetypal structure of the modules from $(311)_{PbS}$-like layers into $(501)_{SnS}$-like ones.

It is important to bear in mind that the choice of rigid-unit rods in the low-pressure lillianite structure is arbitrary. An inspection of Figure 5 shows that the chosen rods (gray) are fully equivalent to the inter-rod spaces (white) in lillianite because of the presence of the mirror planes. It is only after the phase transition that the rigid rods become distinct from the sheared inter-rod spaces. A peculiar structural property of lillianite (and possibly other members of the lillianite homologous series) is that once the shearing planes and rigid rods begin to form in one part of the crystal, the sequence is determined for the rest of the structure and no twin domains appear because no alternative rotations are possible for the rods. This is the reason why the phase transition does not destroy the single crystal.

The structural change resembles the one typically observed during a plastic deformation, but the shear in this case is produced under the hydrostatic conditions and the change is reversible. This can be explained as a result of the LEP stereochemical activity. The SnS-archetype structure obviously allows a volume reduction compared to the PbS-

(27) Berlepsch, P.; Makovicky, E.; Balić-Žunić, T. *Neues Jahrb. Mineral., Monatsh.* **2001**, *3*, 115–135.

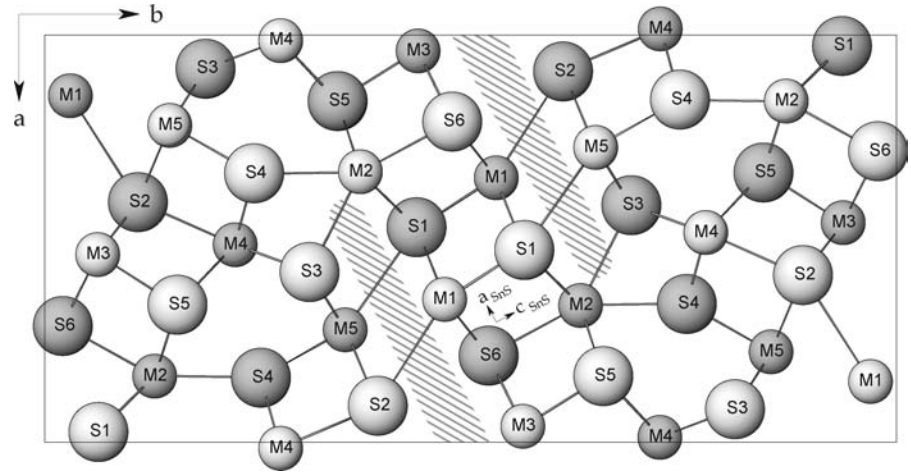

Figure 4. One unit cell from the crystal structure of β-$Pb_3Bi_2S_6$. Gray circles represent atoms on the $z = 0.25$ mirror plane, and white circles represent atoms on the $z = 0.75$ mirror plane. The orientation of the SnS-archetype axes inside one (010) structural slab is indicated. Only M−S contacts under 3.5 Å are drawn. Cores of the LEP micelles are indicated by ruling.

Table 6. Atomic Coordinates for β-$Pb_3Bi_2S_6$ (*lill2* Crystal)

P (GPa)		5.27(4)	7.92(5)
M1	*x*	0.1490(6)	0.1491(6)
	y	0.0297(2)	0.0308(2)
	z	0.250	0.250
M2	*x*	0.3359(6)	0.3359(6)
	y	0.3701(2)	0.3698(3)
	z	0.750	0.750
M3	*x*	0.0396(5)	0.0395(6)
	y	0.4383(3)	0.4395(3)
	z	0.250	0.250
M4	*x*	0.0150(5)	0.0157(6)
	y	0.2781(2)	0.2768(3)
	z	0.750	0.750
M5	*x*	0.2235(5)	0.2249(5)
	y	0.1477(3)	0.1463(3)
	z	0.750	0.750
S1	*x*	0.4790(33)	0.479(4)
	y	0.4392(16)	0.4369(18)
	z	0.250	0.250
S2	*x*	0.398(3)	0.401(3)
	y	0.1106(13)	0.1108(16)
	z	0.250	0.250
S3	*x*	0.083(3)	0.094(3)
	y	0.1845(17)	0.1822(15)
	z	0.250	0.250
S4	*x*	0.338(3)	0.336(3)
	y	0.2378(15)	0.2393(15)
	z	0.750	0.750
S5	*x*	0.165(3)	0.159(3)
	y	0.3451(14)	0.3439(15)
	z	0.250	0.250
S6	*x*	0.223(3)	0.220(3)
	y	0.4774(15)	0.4803(16)
	z	0.750	0.750

Table 7. Atomic Displacement Factors for β-$Pb_3Bi_2S_6$ (*lill2* Crystal)

P (GPa)		5.27(4)	7.92(5)
M1	U_{ef}	0.0160(16)	0.0153(17)
M2	U_{ef}	0.0193(15)	0.0190(17)
M3	U_{ef}	0.0182(15)	0.0165(16)
M4	U_{ef}	0.0188(16)	0.0250(19)
M5	U_{ef}	0.0161(15)	0.0142(16)
S1	U_{iso}	0.012(8)	0.018(9)
S2	U_{iso}	0.000(7)	0.005(8)
S3	U_{iso}	0.018(9)	0.006(8)
S4	U_{iso}	0.015(8)	0.007(7)
S5	U_{iso}	0.003(7)	0.003(7)
S6	U_{iso}	0.011(8)	0.012(8)

Table 8. Cation−Anion Distances (Å) in β-$Pb_3Bi_2S_6$

P (GPa)		5.27(4)	7.92(5)
M1	S1	2.52(4)	2.55(4)
	2 × S6	2.74(2)	2.71(2)
	2 × S1	2.84(2)	2.82(3)
	S2	3.32(3)	3.29(3)
	S3	3.64(4)	3.49(3)
	⟨M1−S⟩	2.95	2.91
M2	S6	2.77(4)	2.81(4)
	2 × S5	2.82(2)	2.84(2)
	2 × S1	3.01(3)	2.96(3)
	S3	3.00(4)	3.05(3)
	S4	3.05(4)	2.96(4)
	⟨M2−S⟩	2.93	2.91
M3	S5	2.55(3)	2.53(3)
	2 × S2	2.79(2)	2.75(2)
	2 × S6	2.99(3)	2.95(3)
	S6	3.49(3)	3.36(3)
	S2	4.03(3)	3.94(4)
	⟨M3−S⟩	3.09	3.03
M4	2 × S4	2.83(2)	2.82(2)
	S2	2.87(3)	2.84(4)
	2 × S5	3.03(3)	2.96(3)
	2 × S3	3.05(3)	3.05(3)
	⟨M4−S⟩	2.95	2.93
M5	S4	2.43(4)	2.43(3)
	2 × S3	2.68(2)	2.59(2)
	2 × S2	2.91(2)	2.88(2)
	S1	3.36(4)	3.28(4)
	S6	3.97(4)	3.81(4)
	⟨M5−S⟩	2.99	2.92

archetype, but at the same time the stereochemical activity of LEPs increases. During the phase transition some of LEPs are transferred to the opposite side of the atomic nuclei and now all are concentrated in the inter-rod spaces. On the release of pressure, it must be the consequent back-migration of LEPs which is the driving force to restore the low-pressure structure. The members of the meneghinite structural family which are stable at low pressures are typically Pb−Sb sulfides, and this example illustrates the differences in the expression and behavior of the s^2 LEPs of Bi and Sb.

The phase transition from lillianite to β-$Pb_3Bi_2S_6$ has several interesting characteristics: it is a first-order, reversible, displacive phase transition with collective migration of chemical bonds, strongly anisotropic, and producing a major volume change. According to these characteristics we propose to call it piezoplastic phase transition. Piezo ($\pi\iota\acute{\varepsilon}\zeta\omega$

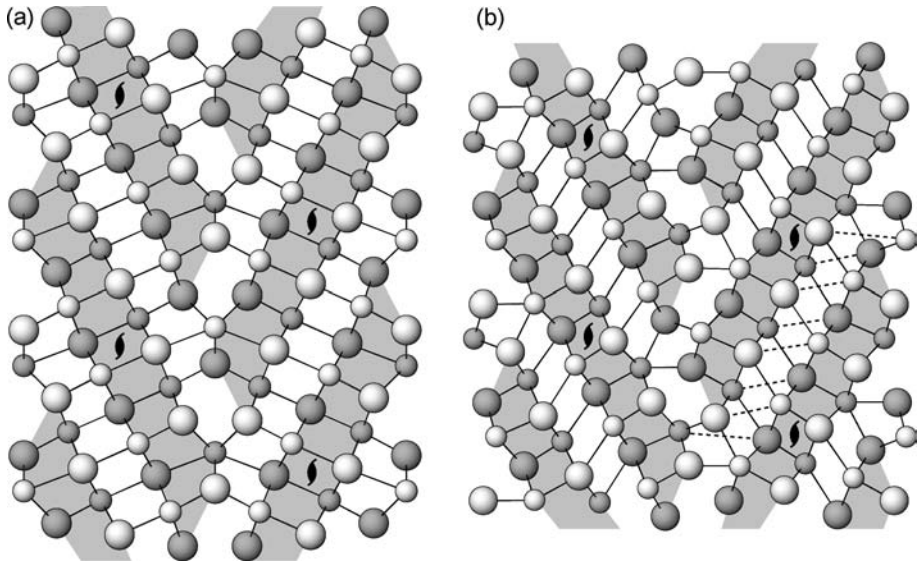

Figure 5. Crystal structure of lillianite (a) and β-$Pb_3Bi_2S_6$ (b). The shaded blocks in (a) become rods in (b). These are rotated and shifted in the process of the phase transition. The dashed lines in (b) indicate the former M−S bonds from the lillianite structure.

= to press) referring to its occurrence under pressure and plastic ($\pi\lambda\alpha\sigma\tau\acute{o}\varsigma$ = molded, formed) referring to the morphological characteristics of the structural change.

The observed phase transition is of special interest because of its high anisotropy combined with reversibility and preservation of the single crystal. It shows that the presence of LEPs on some metal- and semimetal atoms and/or the modular character of the crystal structure can give unique compressional properties to materials. In this respect, the sulfosalts, with their rich structural variation in both respects, could present further interesting examples.

Acknowledgment. This work is supported by the EUROCORES/EuroMinSci project "Ordering of Ions in Minerals" and by a grant from the Danish Natural Science Research Council. We would like to thank the reviewers for constructive comments.

IC800380P